

Exploring the LHC Landscape with Dileptons

DIMITRI BOURILKOV

bourilkov@mailaps.org

*Physics Department, University of Florida, P.O. Box 118440
Gainesville, FL 32611, USA*

Abstract

The dilepton decay channels provide clean signatures and are an ideal hunting ground for high mass resonant, like Z' , or non-resonant, like contact interactions or extra dimensions, searches at the LHC. The production of high invariant mass opposite sign lepton pairs in proton-proton collisions in the Standard Model is dominated by the Drell-Yan process. In addition to this photon or Z exchange mediated mechanism, photons radiated by the incoming protons can collide and produce lepton pairs. In this paper detailed calculations of the Drell-Yan process at next-to-next-to-leading order in QCD and next-to-leading order in the electroweak corrections, augmented with the photon-induced effects, are presented in the typical acceptance of a multi-purpose LHC detector at center of mass energy 13 TeV. Estimates of the expected backgrounds for new physics searches are provided for dilepton invariant masses up to the LHC kinematic limit.

1 Introduction

The Standard Model (SM) of particle physics has ruled the collider scene for decades. Varied and very detailed tests of the SM have confirmed its validity at the available energies. Searches for new physics phenomena beyond the SM in dilepton (electron or muon) final states provide clean signatures and have been a mainstay of the quest strategy. Resonant or non-resonant effects have been searched for extensively at hadron colliders like the LHC, see e.g [1, 2, 3, 4, 5, 6, 7, 8], and in the cleaner environment of lepton colliders at lower energies, see e.g. [9, 10, 11].

The backgrounds for new high mass resonant (like Z') or non-resonant (like contact interactions or extra dimensions) effects are dominated by the Drell-Yan (DY) process of opposite sign lepton pair production, mediated through photon or Z exchange from the initial partons in the incoming protons. With the rapidly increasing accumulated luminosity at the LHC precise estimations of the background are a key ingredient of the dilepton searches, especially of the non-resonant variety. To reach the required precision, calculations at next-to-leading order (NLO) and next-to-next-to-leading order (NNLO) in Quantum Chromodynamics (QCD) are needed. NNLO cross section calculations reduce the dependence of the results on the renormalization and factorization scale choices to the couple of percent level, as expected when enough orders are included in the calculation.

The QCD calculations depend on the parton density functions (PDF) of the protons. The following modern PDFs [12, 13, 14, 15] are used in this study. The PDF uncertainties are estimated using the latest PDF4LHC [16] prescriptions. In most cases the CT14 PDF set, the PDF4LHC15 set (which is an average of the CT14, MMHT14 and NNPDF3.0 PDF

sets) or the LUXqed_plus_PDF4LHC15 set are used. Additional PDF sets are utilized for special purposes. The reweighting technique [17] for PDF uncertainties is used.

Beside the QCD effects, electroweak (EWK) effects become very important at LHC energies. Technically (and as implemented in various calculation or simulation tools), they fall in two classes:

1. Quantum Electrodynamics (QED) only effects: Final State Radiation (FSR), Initial State Radiation (ISR) and their interference
2. Pure Weak corrections: vertex, WW and ZZ box, and self-energy contributions.

In addition to the DY process, lepton pairs can be produced in gamma-gamma collisions, where photons radiated by the incoming protons collide. To calculate this process, usually labeled photon-initiated (PI) background in various searches, we need parton density functions including the photon component. Quantum Electrodynamics introduces corrections to the parton evolution: photon parton distributions $\gamma(x, Q^2)$ are present for the proton (neutron), and part of the proton (or neutron) momentum is carried by the photons. The PDF depends on the parton momentum fraction - Bjorken x , and the momentum transfer Q^2 . In this study the modern photon PDFs [15, 18] are used. In Drell-Yan, W and Z production at the LHC the photon contribution is suppressed by a factor $\mathcal{O}(\alpha/\alpha_s)$ compared to the canonical quark-antiquark contribution.

For an up-to-date paper on the issues involved in precision studies of the DY process, see e.g. [19], which concentrates on W and Z boson production. In contrast, the focus of this paper is on the high mass search region up to the LHC kinematic limit - a not so well explored area of phase space.

2 Setup

The calculations for the Drell-Yan process and the photon-induced background are carried out with the program FEWZ [20]. The G_μ scheme with the W mass, the Z mass and the Fermi constant G_μ (measured in muon decay) as input parameters besides the fermion masses is used. The strong coupling is set to $\alpha_s(M_Z) = 0.118$. The PDFs considered in this study are CT14, NNPDF30, PDF4LHC15 and LUXqed_plus_PDF4LHC15, as provided by the LHAPDF libraries version 5 or 6 [21, 22, 23].

Full electroweak corrections at next-to-leading order (NLO) are computed (the flag `EW control = 0` is used). QCD effects are computed at next-to-leading order (NLO) and next-to-next-to-leading order (NNLO). When the PI background is added to the Drell-Yan cross section we label the results DY+PI.

Calculations for dielectrons or dimuons in the acceptance of a generic general purpose LHC experiment are presented: both outgoing leptons are required to have pseudorapidity $|\eta| < 2.4$. Relatively hard cuts suitable for searches at high invariant masses extending to the multi-TeV region are used - the transverse momenta for both leptons have to satisfy $p_T > 50$ GeV.

An important difference between the two channels is the treatment of photons located close in space to the leptons. They can originate from Final State Radiation, or from unrelated sources, e.g. the copious decays of π^0 in a hadron collider environment. The

variable ΔR is used to measure “closeness”:

$$\Delta R = \sqrt{(\Delta\eta)^2 + (\Delta\varphi)^2}, \quad (1)$$

where η and φ are the pseudorapidities and azimuthal angles of the lepton and the photon.

In the case of electrons the electromagnetic calorimeters of the experiments provide a natural “integration” of the energies of close-by photons with the electron energies. As a result the invariant mass reconstructed from the electron energies is closer to the electron pair mass before FSR. In the case of muons where the transverse momenta can be measured both in the central trackers, and in the outer muon detectors after the photons are absorbed, there is no such effect. Two lepton definitions as available in FEWZ are used in the calculations:

1. “Dressed” electrons: photons within $\Delta R < 0.1$, and with $|\eta| < 2.5$ and transverse momentum $p_T > 0.5$ GeV are included in the electron energies
2. “Bare” muons: photon energy is not included.

The CT14qed set is introduced in [18]. The initial photon distribution is defined by the initial photon momentum fraction

$$p_0^\gamma = \int_0^1 x f_{\gamma/p}(x, Q_0) dx \quad (2)$$

at scale $Q_0 = 1.295$ GeV.

From the ZEUS data on deep inelastic scattering with isolated photons [24] the photon PDF is constrained to $p_0^\gamma \leq 0.14\%$. The constraint can be improved in measurements where the photon contribution is enhanced by selecting exclusive dimuon pair production in elastic, single dissociative and double dissociative pp collisions [25, 26]. These CMS measurements are used in [27] to update the CT14qed analysis:

$$p_0^\gamma \leq 0.09\% \text{ at } 68\% \text{ CL} \quad (3)$$

$$p_0^\gamma \leq 0.13\% \text{ at } 90\% \text{ CL} \quad (4)$$

consistent with the ZEUS data analysis.

Recent developments determine the photon PDFs to even higher precision. The importance of taking into account both the coherent (photon emission from the proton as a whole) and non-coherent components in the initial photon distribution is highlighted in [28], and a well determined photon PDF is obtained for high mass lepton pair production. A model-independent approach [15] looks in great detail at the photon distribution, and constrains it quite well with electron-proton scattering data. The result is the LUXqed_plus_PDF4LHC15 photon PDF set.

3 Cross Section Calculations

EWK corrections

In Figure 1 the cross section ratios at NLO in QCD and electroweak corrections are shown. We compare three sets of calculations:

1. QCD at NLO, no EWK corrections
2. QCD at NLO and QED corrections: FSR, ISR and their interference; Weak corrections off
3. QCD at NLO and full EWK corrections.

As can be seen the pure QED corrections are bigger in the dimuon channel due to the use of “bare” muons. The full EWK corrections are very important at high invariant masses: they reduce the cross section by more than 20% in the dielectron channel and by up to 30 % in the dimuon channel. In some Monte-Carlo simulations only QED effects are taken into account. Clearly the inclusion of full EWK effects is key for successful comparisons to data. The importance of complete EWK corrections for LHC at 14 TeV was recognized early [29]. The results presented here agree well with calculations in this exploratory study. Higher order corrections of mixed QCD-EWK type $\mathcal{O}(\alpha_s\alpha)$ are ignored in FEWZ. They are generally less important [30] except for high precision studies.

PDF uncertainties

In Figure 2 the PDF uncertainties for the NLO cross sections (QCD and full EWK), using the CT14nlo PDF, are shown as a function of mass. They become sizable above 2 TeV and approach $\sim \pm 40\%$ for masses above 5 TeV. As discussed later, the PDF uncertainties are dominant at high mass.

PDF choice

The dependence of the cross sections on the choice of PDF is displayed in Figure 3A for the CT14nlo and PDF4LHC_nlo_100 sets. For masses below 5 TeV the variation is below 5%, reaching $\sim 15\%$ for the highest masses. The variation from one is covered by the PDF uncertainties, and could become important only for very high integrated luminosities - as shown in the next section even for 100 fb^{-1} no events from SM sources are expected above 5 TeV.

α_s dependence

In Figure 3B the dependence of the cross sections on variations in the value of the strong coupling constant α_s is examined. For variations larger than the current error from the world average [31]:

$$\alpha_s(M_Z) = 0.1185 \pm 0.0006, \tag{5}$$

the effects are below 1% for the whole mass range under study.

PI background

The effect of photon-initiated lepton pair production on the cross sections is shown in Figure 4, where the ratios $(DY+PI)/DY$ are displayed. The CT14qed_proton PDF is used. It includes the photon contribution. The initial photon momentum fraction p_0^γ ,

which is a free parameter, is varied between 0.00% and 0.09% as discussed earlier, and the two limiting cases are displayed. Their difference is used as one standard deviation in the first event rates estimate.

The recent photon PDFs, publicly available as of this writing, are compared in Figure 5 for the dimuon channel. The CT14qed_inc_proton PDF is based on CT14nlo with the initial photon PDF defined by the sum of the inelastic photon PDF and the elastic photon PDF, obtained from the equivalent photon approximation. The inclusion of the elastic component enhances the PI contribution. The results from the LUXqed_plus_PDF4LHC15 set show the highest PI effects ¹. This set is used for the second estimate of event rates. It benefits also from smaller PDF uncertainties at NNLO, see Figure 5.

The photon-initiated effects are generally small, not above the 5% level for masses of up to ~ 2 TeV, and can reach ~ 15 – 20% above 5 TeV if the photon momentum fraction is taken to be 0.09% or if the LUXqed_plus_PDF4LHC15 set is used. The one σ band defined above for CT14qed_proton PDF is also shown in Figure 5. The predictions from the CT14qed_inc_proton PDF are inside this band for masses above 1.5 TeV, while for the LUXqed_plus_PDF4LHC15 set they fall inside the band only for the highest masses. The newest photon PDFs predict somewhat stronger PI effects in the lower half of the mass range under study.

The results presented here agree well with the results from [32] based on the pioneering MRST2004qed [33] PDF set. The predictions from the freely parametrized NNPDF photon PDF [34], also analyzed in [32], and the newer version [35], have large PDF uncertainties in the most interesting search region².

NNLO/NLO K functions and NNLO PDF uncertainties

In Figure 6 the cross section ratios for calculations at NNLO or NLO in QCD, the so called K functions, are shown for dielectrons and dimuons. In all cases full EWK corrections are included. The K functions are below 1.04 for the whole mass range under study, so the NNLO QCD effects are quite small. The K functions exhibit a complex behavior as a function of mass.

Figure 7 compares the PDF uncertainties for NLO and NNLO cross sections (QCD and full EWK), using the order-matched CT14nlo and CT14nnlo PDFs. The good news is that the uncertainties are reduced at NNLO.

Scale dependence

If enough orders are included in the perturbative expansion, the results should not depend on the choice of renormalization and factorization scales. Traditionally this effect is estimated by varying the scales by a factor of two around the nominal scale, which for Drell-Yan is taken to be the mass of the outgoing dilepton system. An example of such variation for NNLO calculations is shown in Figure 8. The cross sections change by less than 3% below masses of 5 TeV. For the highest masses the variation reaches 3.6%. At NNLO in QCD the calculations are precise enough to serve the needs of searches for new phenomena.

¹The results for lepton pair production with LUXqed_plus_PDF4LHC15 are close to the results from [28].

²Subsequent studies are confirming these conclusions, see e.g. [36].

All combined

In Figure 9 the K functions and photon-induced effects are combined. The ratios of NNLO cross sections including PI contributions to NLO cross sections (QCD and full EWK) are shown, using the CT14 PDF sets. Results with all effects taken into account will be discussed in the rest of this paper.

4 Differential Cross Sections and Event Yields

The differential cross sections as function of mass are shown in Figure 10 for the dielectron and dimuon channels. The CT14 PDFs are used for the first set of results. The uncertainty of the photon-induced background, as defined in the previous section, can be seen on the plots. As this background is much smaller than the Drell-Yan contribution, the impact on the combined cross section is minor.

Ad-hoc fits to the differential cross sections as function of mass are shown in Figure 11. The following function is used:

$$\frac{d\sigma}{dm} = p_0 \cdot m^{(p_1 + p_2 \cdot \ln m + p_3 \cdot (\ln m)^2 + p_4 \cdot (\ln m)^3)}, \quad (6)$$

where p_0 to p_4 are free parameters, m is the invariant mass of the dilepton system in TeV, and σ is the cross section in fb. The fits, inspired by the “not-too-far from linear” behavior of the curves on a double logarithmic plot, perform well if five parameters are used. The $\chi^2/\text{d.o.f.}$ is good, and the fit parameters are shown on the plots for the two channels. The shapes of the two distributions are identical within the statistical errors, while the yield (compare the values of the p_0 parameter) is higher in the electron channel, as discussed in the next paragraph.

The cumulative numbers of events, expected in one experiment above a given mass for integrated luminosity of 100 fb^{-1} at 13 TeV, are given in Figure 12 for the two channels. The apparent “kink” in the distributions at 1 TeV is just an artifact of the change of binning from 0.1 to 0.5 TeV bins at this point. The expected numbers of events are summarized in Table 1. The yield is slightly higher in the dielectron channel due to the recovery of FSR radiation by the electromagnetic calorimeters. As a result fewer events migrate to lower masses. In practice, this channel has an additional advantage due to the favorable energy dependence of the mass resolution. In the dimuon channels the mass resolution relies on tracking and deteriorates at high mass. All things being equal the dielectron channel might be first in a discovery. Additional search options are provided by measuring the forward-backward asymmetry. Here the muon channel may have an advantage, as the charge determination for electrons relies on the central trackers with much shorter lever arm, so it becomes increasingly difficult at high energies. Around one event with mass exceeding 3 TeV per channel is expected for luminosity of 100 fb^{-1} . Given the luminosities being collected by ATLAS and CMS in 2016, with a bit of luck we may expect to see first event(s) at these high masses this year.

The event yields are reproduced well by integrating the fits to the differential cross sections, shown in Figure 11. The “From Fit” columns in Table 1, obtained this way, agree with the yields produced by calculating directly from the cross sections (the “Events” columns). All that is needed for predictions in different binnings is a new integration of the fit functions.

Table 1: Cumulative expected numbers of events in one experiment above a given mass for integrated luminosity of 100 fb^{-1} at 13 TeV, using the CT14 PDF sets. The “From Fit” columns are obtained by integrating the fits to the differential cross sections, as explained in the text. All effects (NNLO and PI) are included.

Mass (TeV)	Dielectrons CT14				Dimuons CT14			
	Events	Error ⁺	Error ⁻	From Fit	Events	Error ⁺	Error ⁻	From Fit
0.4	17500	215	282	17600	16950	210	274	17050
0.5	8100	99	131	8090	7820	97	127	7800
0.6	4180	53	69	4200	4030	51	67	4040
0.7	2340	32	42	2370	2240	31	40	2280
0.8	1380	22	28	1420	1320	21	27	1360
0.9	850	17	22	890	810	16	21	850
1.0	540	15	19	570	520	14	18	550
1.5	81.0	2.7	3.2	87.5	76.7	2.6	3.1	82.9
2.0	16.8	0.68	0.78	17.9	15.8	0.64	0.74	16.8
2.5	4.1	0.21	0.23	4.3	3.8	0.20	0.22	4.0
3.0	1.1	0.073	0.077	1.1	1.0	0.062	0.064	1.0
3.5	0.33	0.027	0.027	0.32	0.30	0.023	0.023	0.29
4.0	0.097	0.0091	0.0091	0.094	0.088	0.0084	0.0083	0.086
4.5	0.029	0.0034	0.0034	0.029	0.026	0.0029	0.0029	0.026
5.0	0.0086	0.0012	0.0012	0.0085	0.0078	0.0011	0.0011	0.0078
5.5	0.0024	0.0005	0.0005	0.0021	0.0022	0.0005	0.0005	0.0019

The total number of expected events above 0.4 TeV for the two channels in one experiment for 100 fb^{-1} is 34450. It is interesting to compare this number to the early study [29] from 1999. The center-of-mass energy is 14 TeV, and the selection is not exactly the same: $|\eta| < 2.5$ and $p_T > 20 \text{ GeV}$ for both leptons. The simulation is done at leading order with PYTHIA 5.7 and the then available PDFs. Given all these caveats, the 1999 prediction: 33000 expected events, is surprisingly close to the new result ³.

The cumulative numbers of events for the two channels, expected in one experiment above a given mass for integrated luminosity of 100 fb^{-1} at 13 TeV, are given in Table 2 using the LUXqed_plus_PDF4LHC15_nnlo_100 set. This PDF set includes both the NNLO and PI effects. As can be seen, the yields agree quite well within the uncertainties with the yields in Table 1 based on the CT14 PDF sets. The LUXqed_plus_PDF4LHC15 set has smaller overall uncertainties and tends to predict slightly higher rates, with both the PI effects and the underlying NNLO PDF set contributing to the enhancement. The event yields are reproduced well by integrating the fit to the differential cross section, shown in Figure 13. The smaller uncertainties in this case result in a somewhat larger

³For the sake of full disclosure, the author of the present paper and the person who produced these numbers back then are identical.

$\chi^2/\text{d.o.f.}$ Within errors the five parameters from the fit agree with the results using CT14, cf. Figure 11.

Table 2: Cumulative expected numbers of events in one experiment above a given mass for integrated luminosity of 100 fb^{-1} at 13 TeV, using the LUXqed_plus_PDF4LHC15 PDF set. The ‘‘From Fit’’ columns are obtained by integrating the fits to the differential cross sections, as explained in the text. All effects (NNLO and PI) are included.

Mass (TeV)	Dielectrons LUXqed_plus_PDF4LHC15				Dimuons LUXqed_plus_PDF4LHC15			
	Events	Error ⁺	Error ⁻	From Fit	Events	Error ⁺	Error ⁻	From Fit
0.4	17760	135	152	17870	17210	131	148	17330
0.5	8230	64	70	8220	7960	63	68	7940
0.6	4270	35	37	4280	4110	34	36	4130
0.7	2390	21	22	2420	2300	21	22	2330
0.8	1410	15	15	1450	1360	14	15	1400
0.9	870	12	12	910	840	11	11	870
1.0	560	10	10	590	530	9.8	9.7	560
1.5	84.3	1.9	1.7	90.7	80.0	1.8	1.6	86.1
2.0	17.6	0.46	0.40	18.7	16.6	0.43	0.37	17.6
2.5	4.4	0.13	0.11	4.5	4.1	0.12	0.11	4.2
3.0	1.2	0.039	0.037	1.2	1.1	0.036	0.034	1.1
3.5	0.35	0.013	0.014	0.35	0.33	0.012	0.013	0.32
4.0	0.11	0.0049	0.0054	0.11	0.098	0.0046	0.0049	0.097
4.5	0.033	0.0021	0.0023	0.033	0.030	0.0019	0.0021	0.030
5.0	0.010	0.0009	0.0011	0.010	0.0092	0.0009	0.0010	0.0092
5.5	0.0029	0.0005	0.0006	0.0026	0.0027	0.0005	0.0005	0.0023

The most important test for the expected yields is the comparison to the data from the LHC experiments. The ATLAS collaboration observes [7] 26 events above 0.9 TeV for integrated luminosity 3.2 fb^{-1} . Corrections have to be applied to this number to account for background contamination and detection efficiency, which work in opposite directions. The ATLAS acceptance extends to $|\eta| < 2.5$, but excludes the transition region $1.37 < |\eta| < 1.52$ between the central and forward calorimeters. The prediction from the numbers in Table 1, rescaled by luminosity and pseudorapidity acceptance, is 26.6 events, in excellent agreement with the data. The comparison in the muon channel is not so straightforward due to the lower detection efficiency and higher backgrounds. The updated preliminary ATLAS dielectron numbers [8] for 13.3 fb^{-1} are 99 observed events. From the results presented here the expectation is 111 events, in good agreement with the data.

A 2.9 TeV event in the dielectron channel observed by CMS [3] is the highest mass event as of this writing. From the numbers in Table 1 and the luminosity reported in the Run 2 papers cited here, the expectation is for ~ 2 events above 2.5 TeV to be observed

when combining the ATLAS and CMS yields in the dielectron and dimuon channels.

5 Outlook

The production of high invariant mass opposite sign lepton pairs in proton-proton collisions at the LHC is an important search region for manifestations of new physics, and for tests of the Standard Model at highest momentum transfers. In this paper the Drell-Yan and photon-induced backgrounds for dilepton searches are examined in great detail. Electroweak corrections, PDF uncertainties and choice, α_s and scale dependencies, and QCD effects at next-to-next-to-leading order are considered. The Drell-Yan background is dominating at high masses, and the major source of uncertainty comes from the limited knowledge of parton density functions in this kinematic area. The photon-induced background plays a supporting role. The backgrounds are low and well understood in the most promising search region, and the LHC accelerator and the experiments are delivering and recording record luminosities. The hunt is on.

Acknowledgments

The author thanks Valery Khoze for very productive discussions.

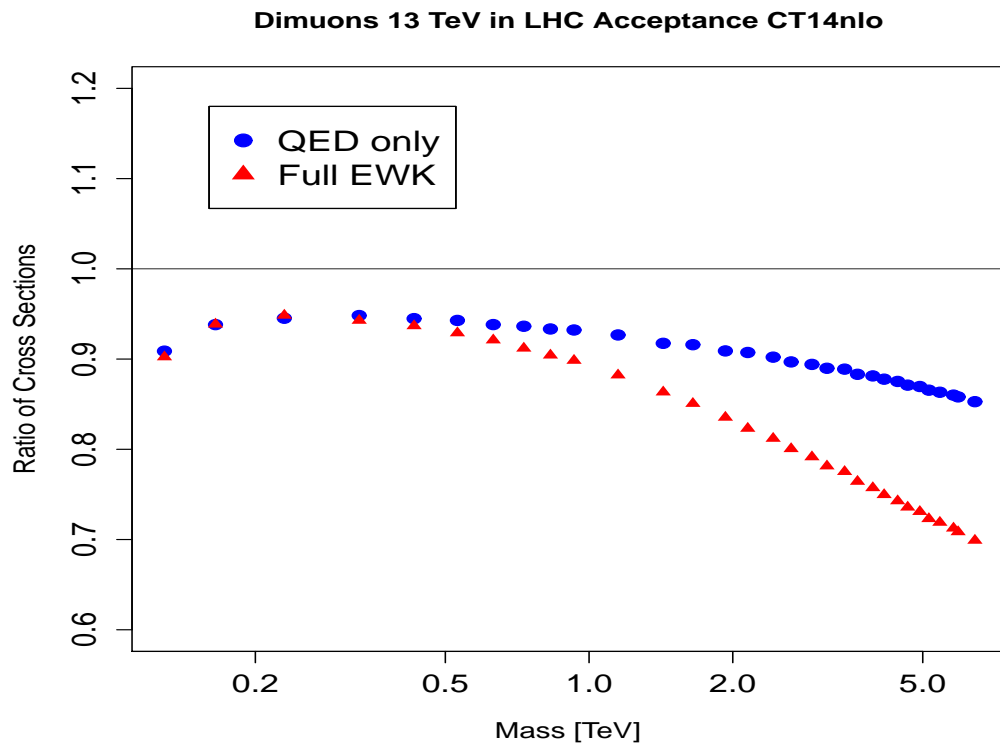
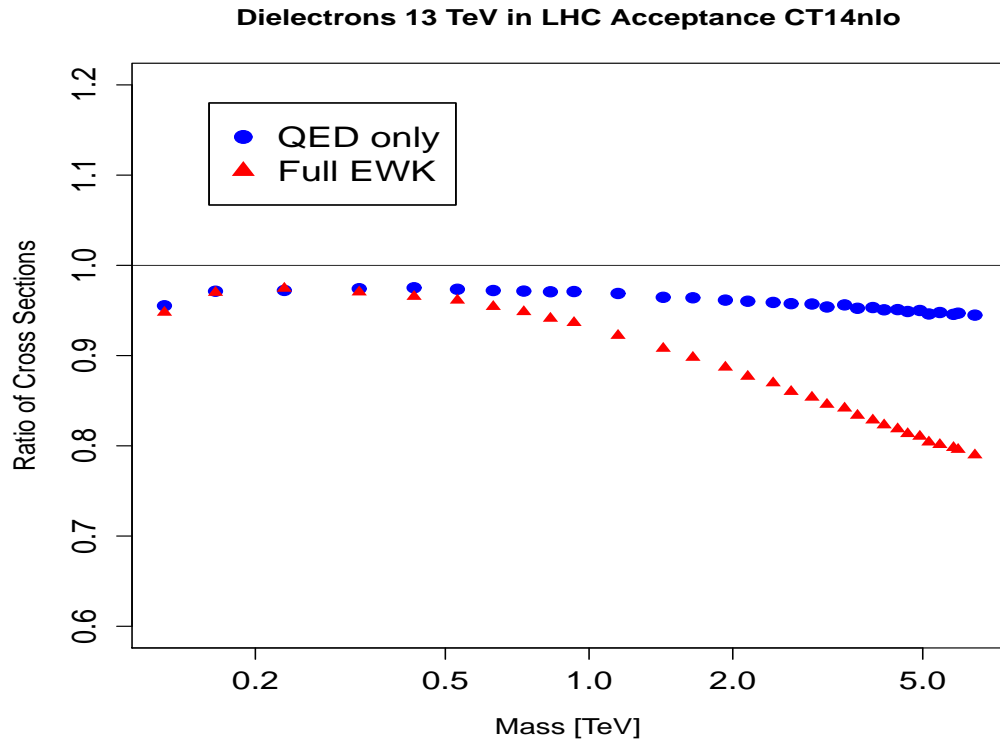


Figure 1: Top: Electroweak corrections for the dielectron channel: QED only and full EWK corrections. Bottom: Electroweak corrections for the dimuon channel: QED only and full EWK corrections.

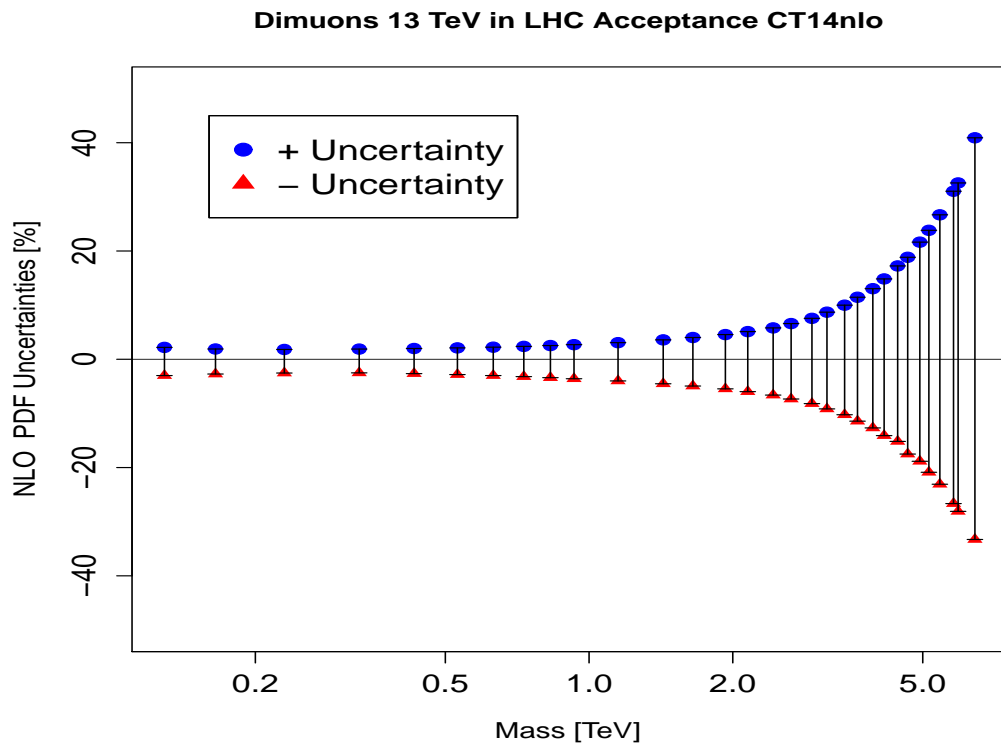
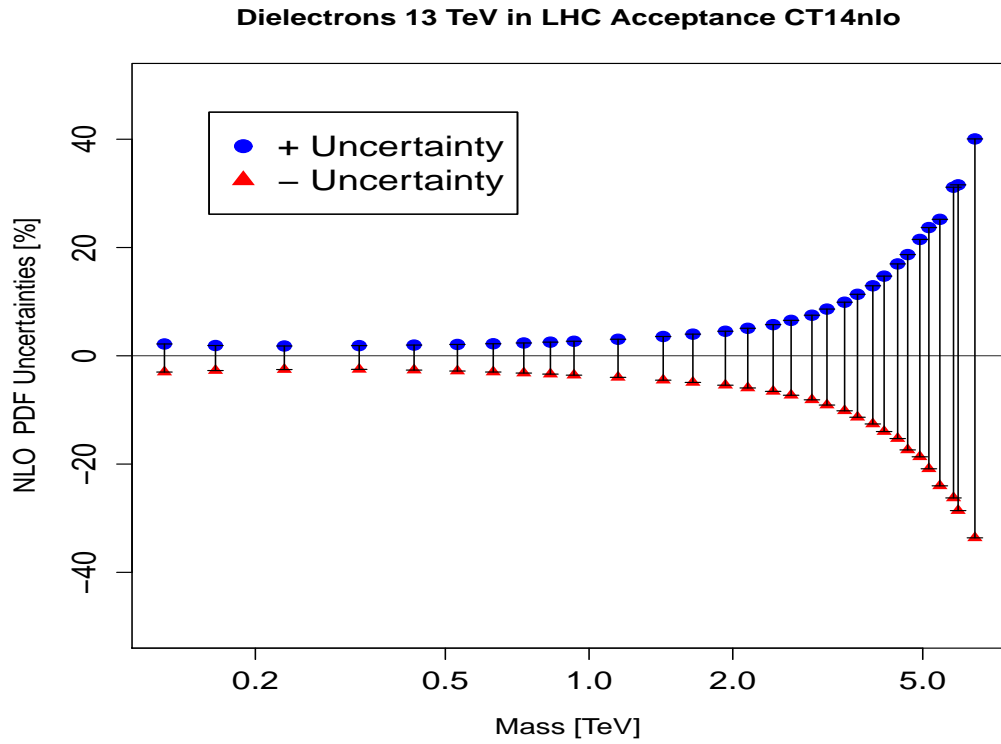


Figure 2: Top: NLO PDF uncertainties for the dielectron channel. Bottom: NLO PDF uncertainties for the dimuon channel.

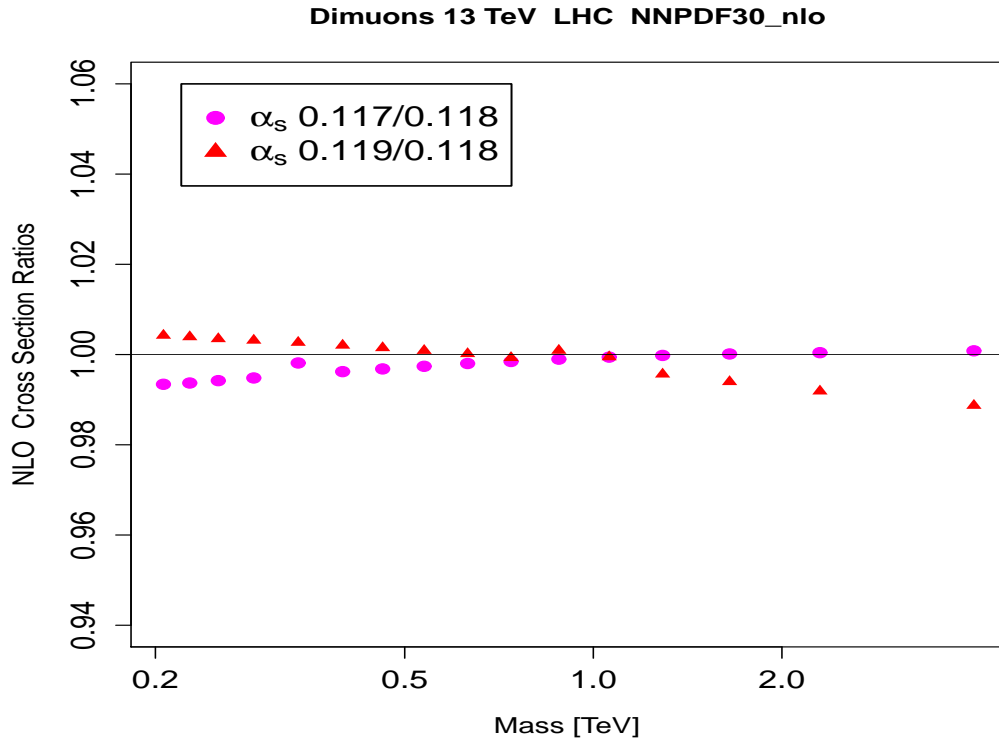
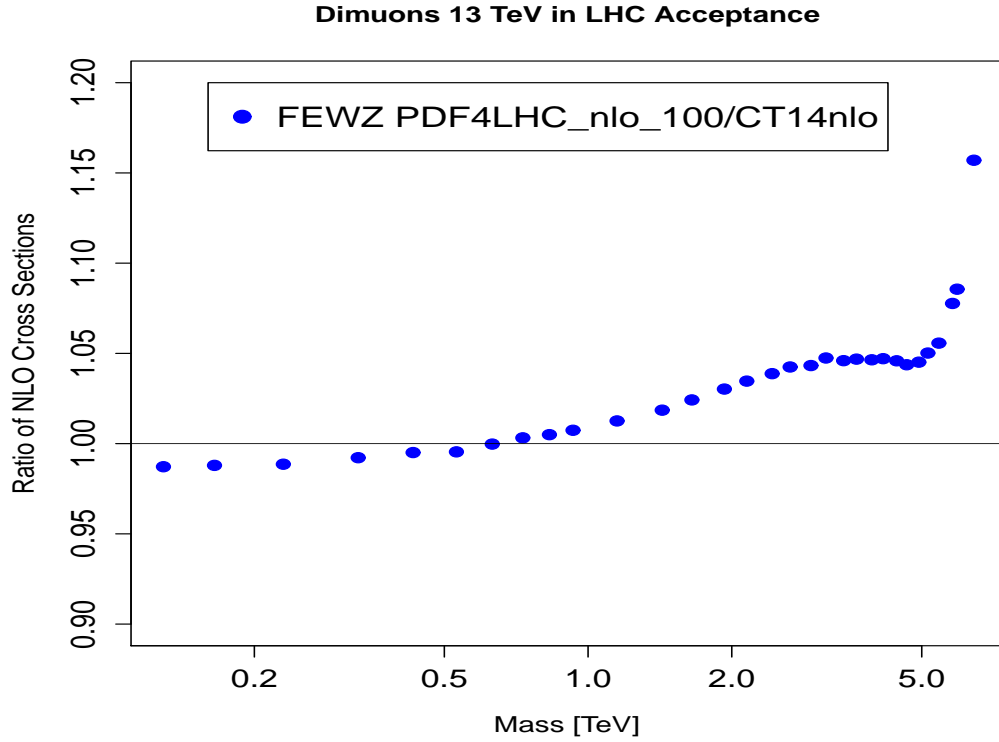


Figure 3: A: Dependence of the cross sections on the choice of PDFs for the dimuon channel. The CT14nlo and PDF4LHC_nlo_100 sets are compared. B: Dependence of the cross sections on variations in the value of the strong coupling constant α_s for the dimuon channel.

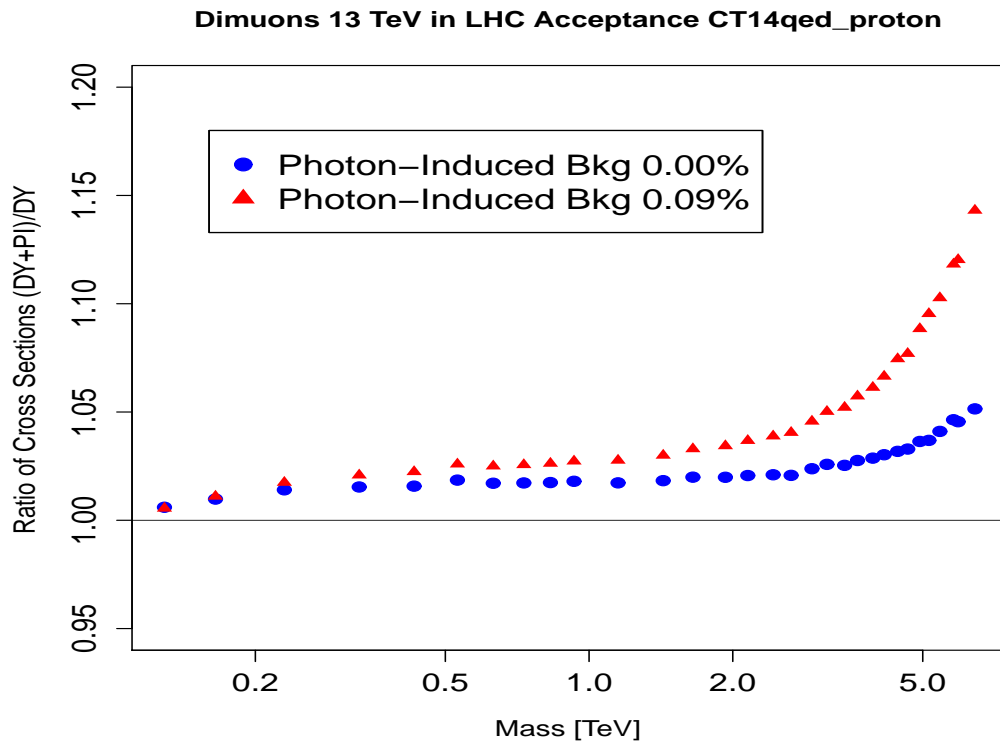
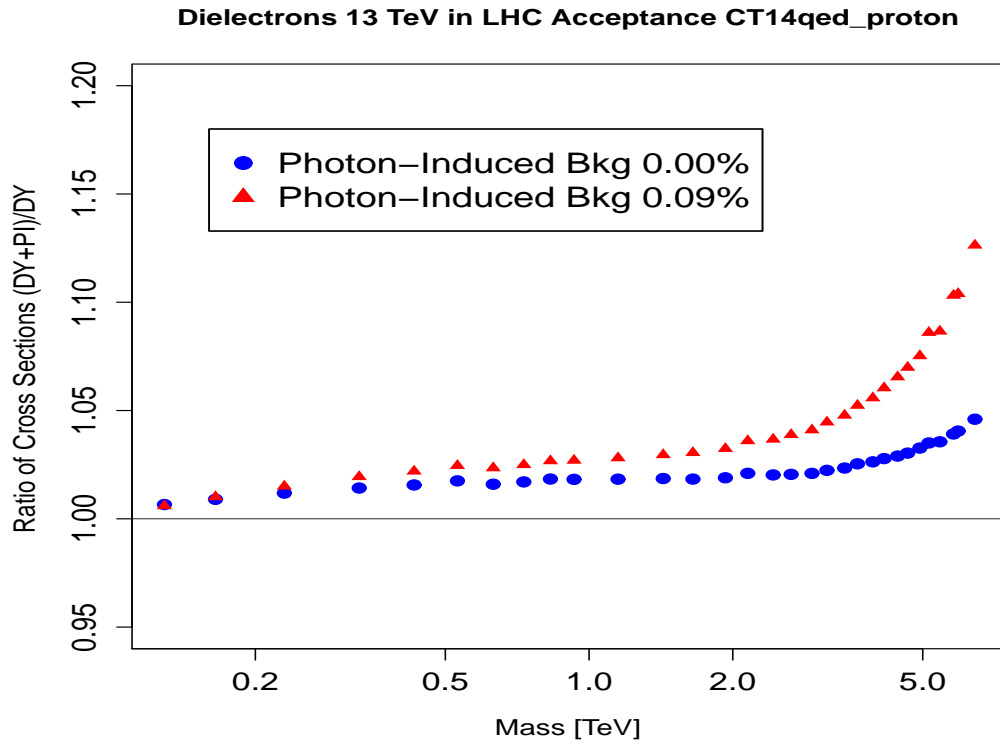


Figure 4: Top: Photon-induced background for the dielectron channel. Bottom: Photon-induced background for the dimuon channel. The cross section ratios $(DY+PI)/DY$ are displayed.

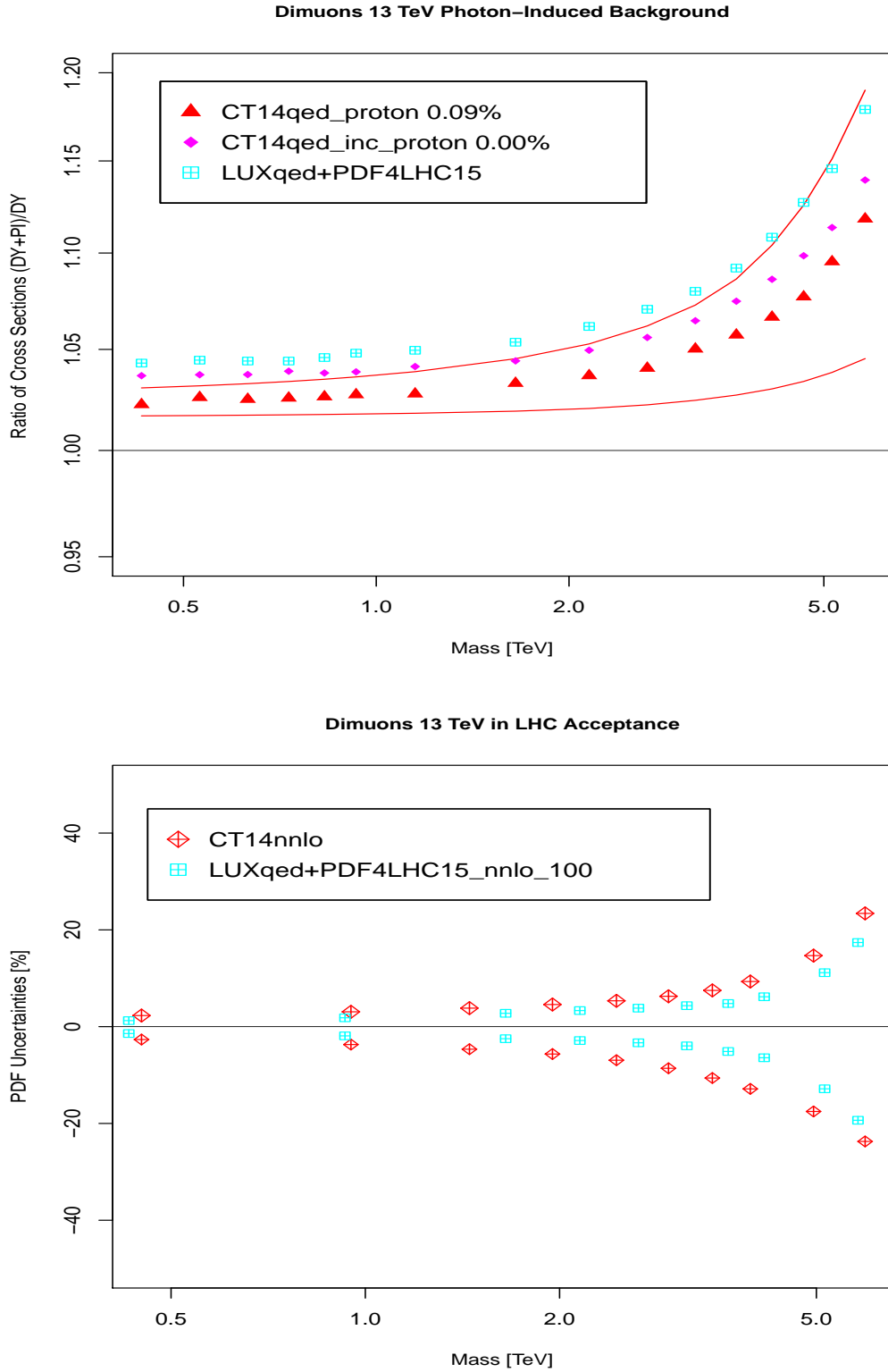


Figure 5: Top: Photon-induced background for the dimuon channel. The cross section ratios $(DY+PI)/DY$ are displayed. The lines represent the one σ uncertainty band for CT14qed_proton, as described in the text. Bottom: NNLO PDF uncertainties for the dimuon channel with CT14nnlo and LUXqed_plus_PDF4LHC15_nnlo_100.

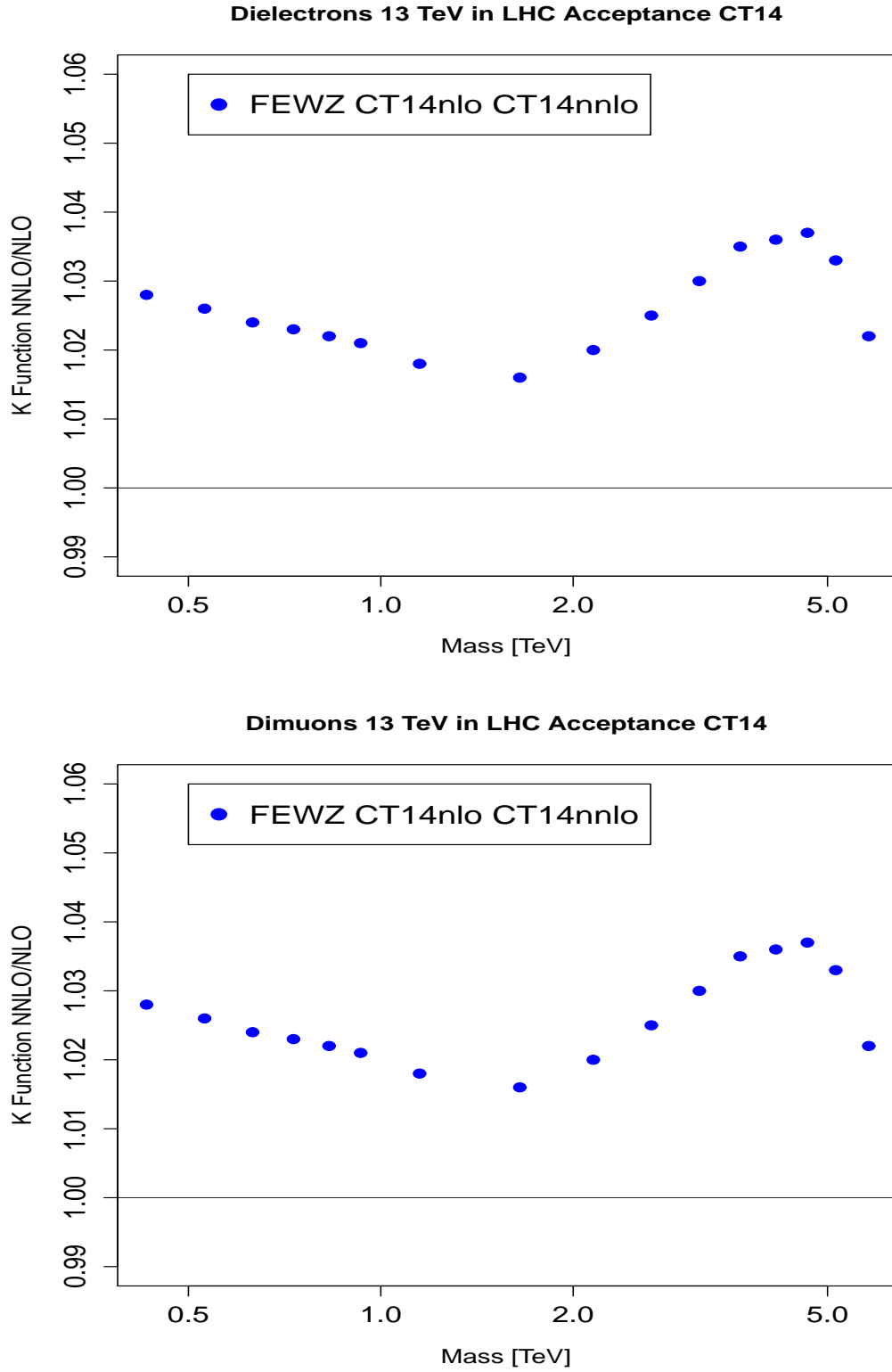


Figure 6: Top: K function NNLO/NLO for the dielectron channel. Bottom: K function NNLO/NLO for the dimuon channel.

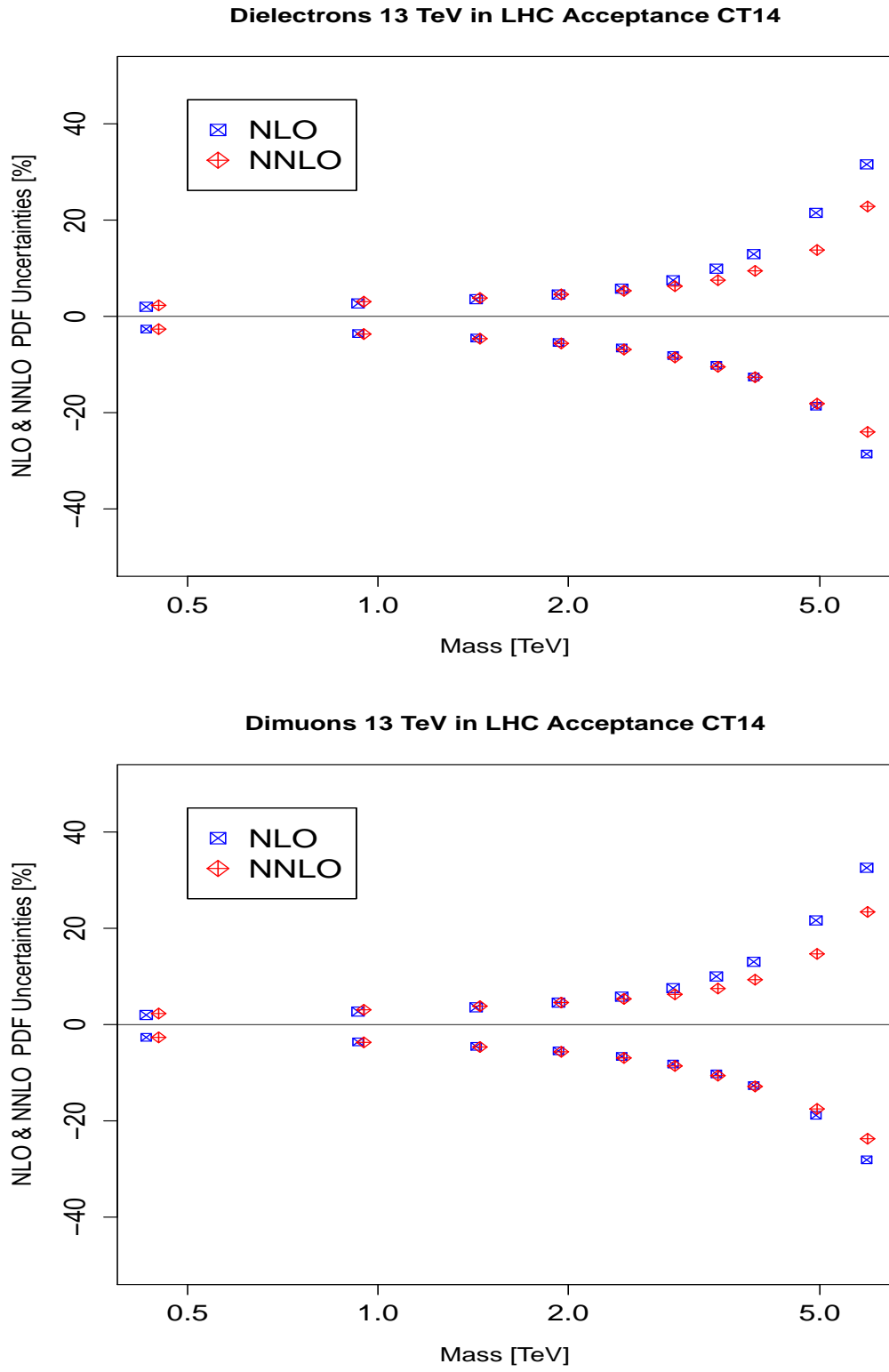


Figure 7: Top: NLO and NNLO PDF uncertainties for the dielectron channel. Bottom: NLO and NNLO PDF uncertainties for the dimuon channel.

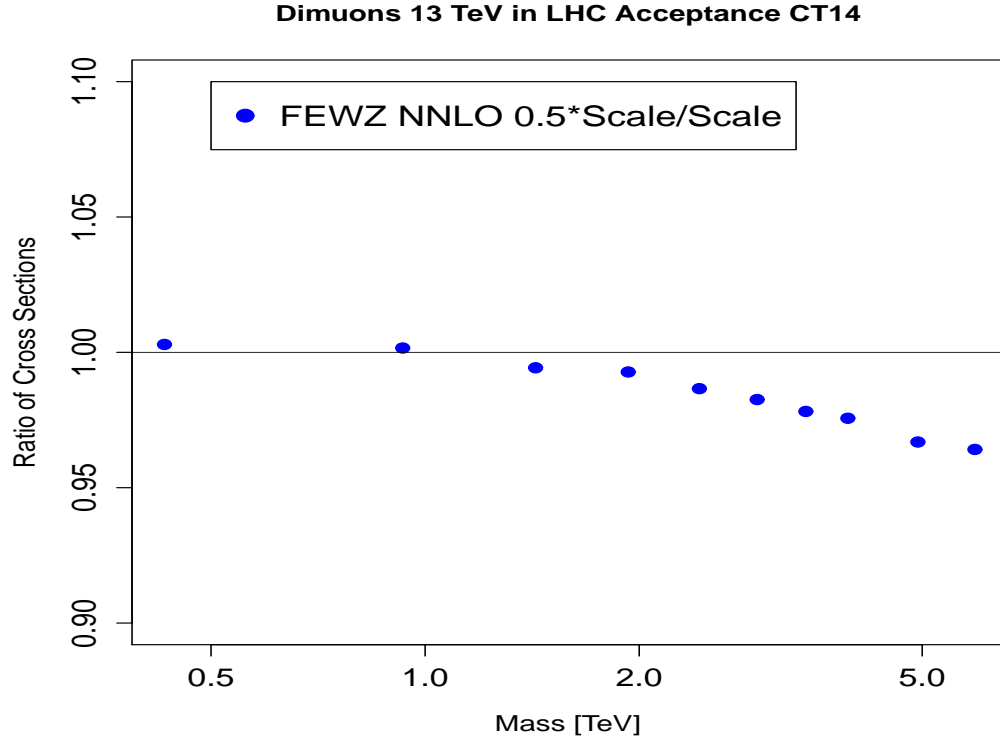


Figure 8: Dependence of the cross sections on the choice of renormalization and factorization scales for the dimuon channel.

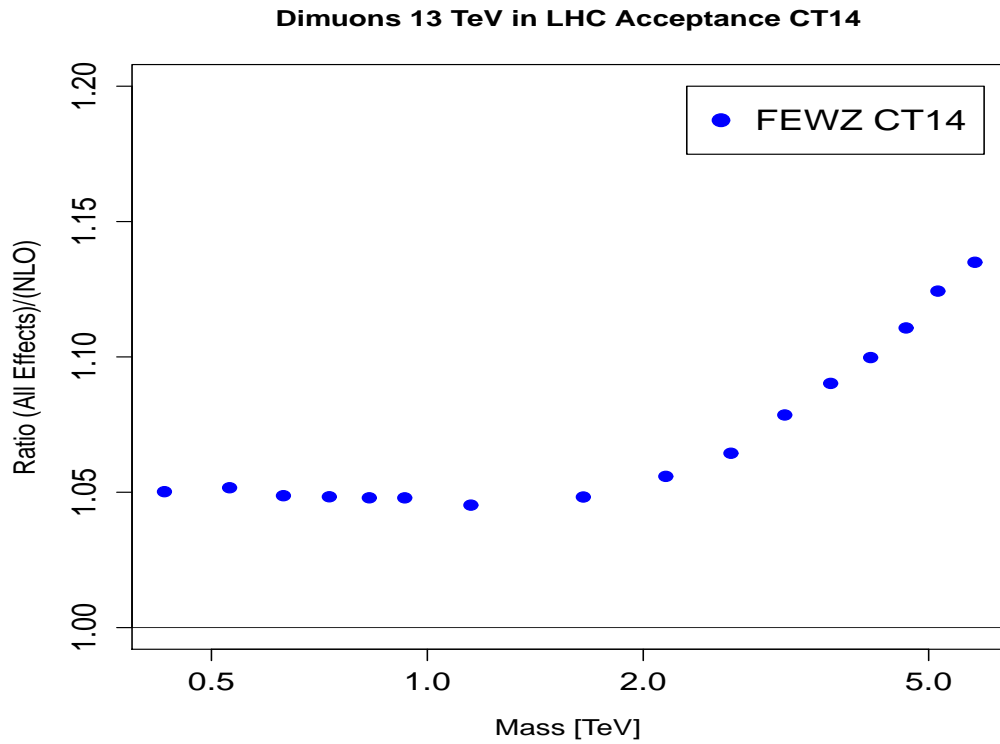
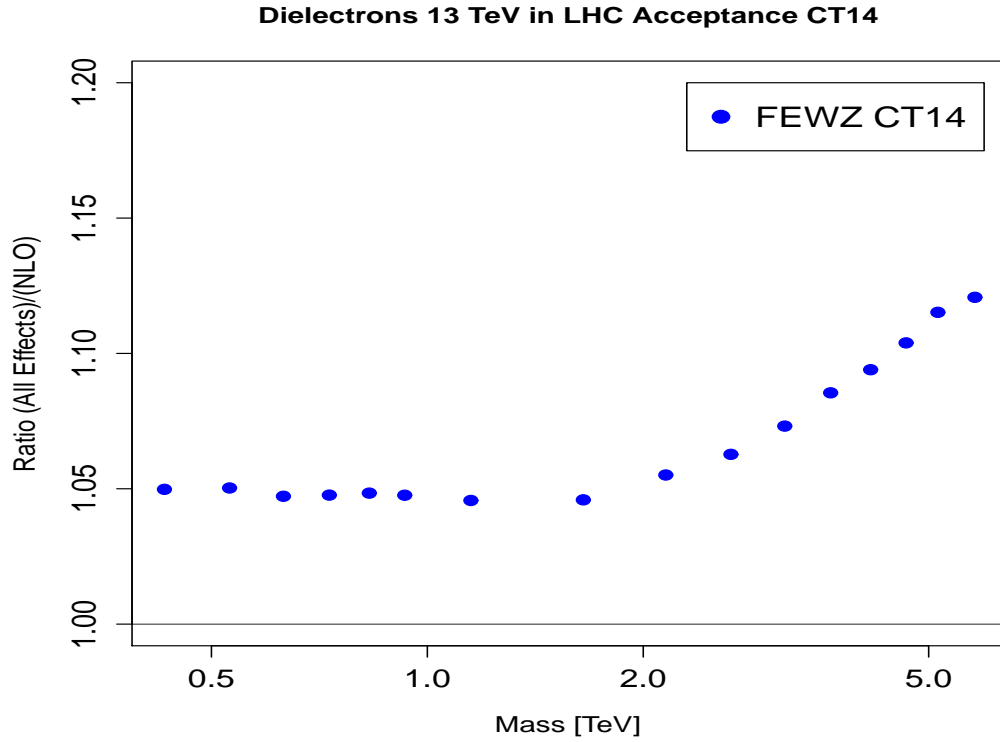


Figure 9: Top: Ratio of cross sections including all effects (NNLO and PI) to NLO cross sections for the dielectron channel. Bottom: Ratio of cross sections including all effects (NNLO and PI) to NLO cross sections for the dimuon channel.

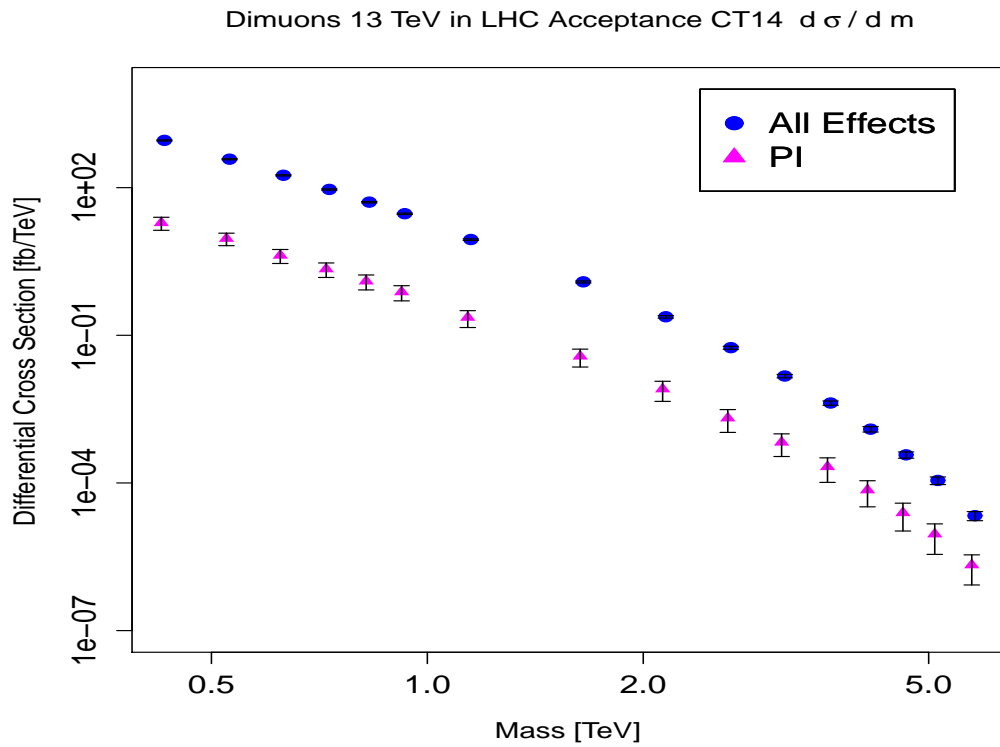
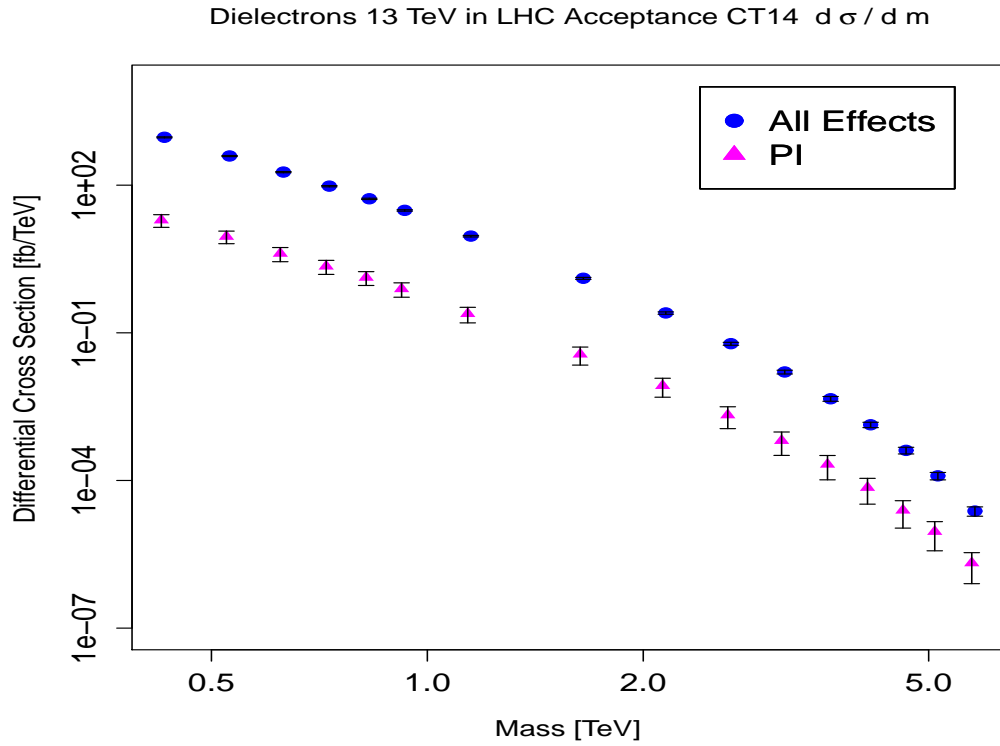


Figure 10: Top: Differential cross section including all effects (NNLO and PI) for the dielectron channel. Bottom: Differential cross section including all effects (NNLO and PI) for the dimuon channel.

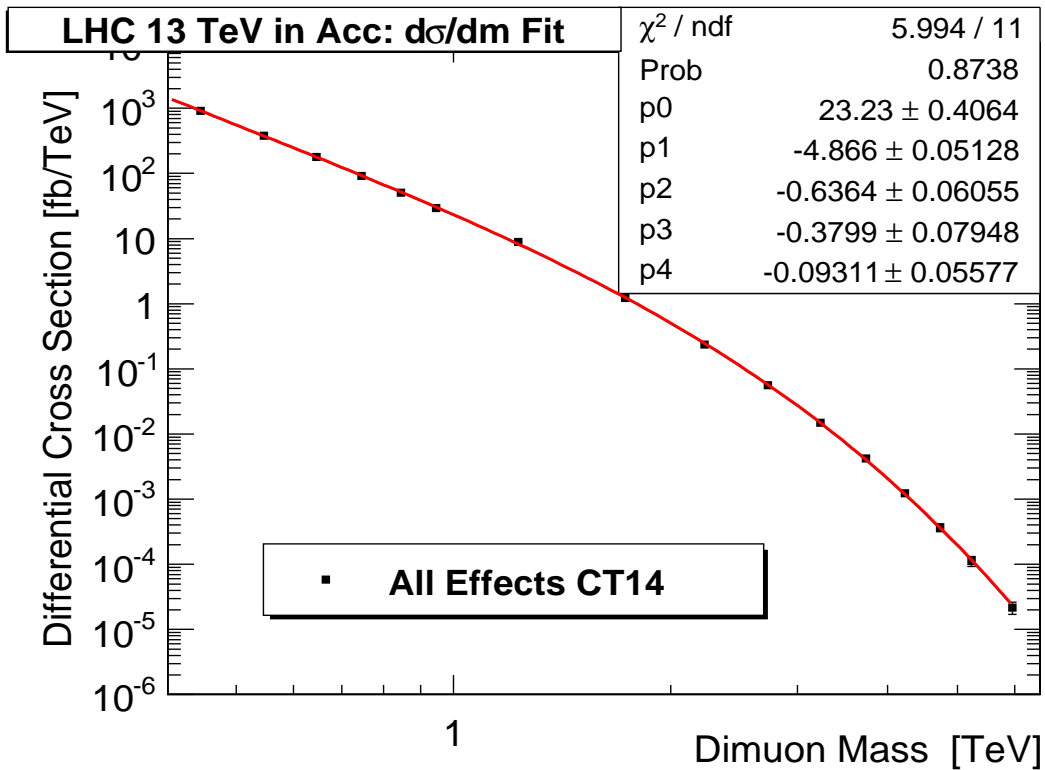
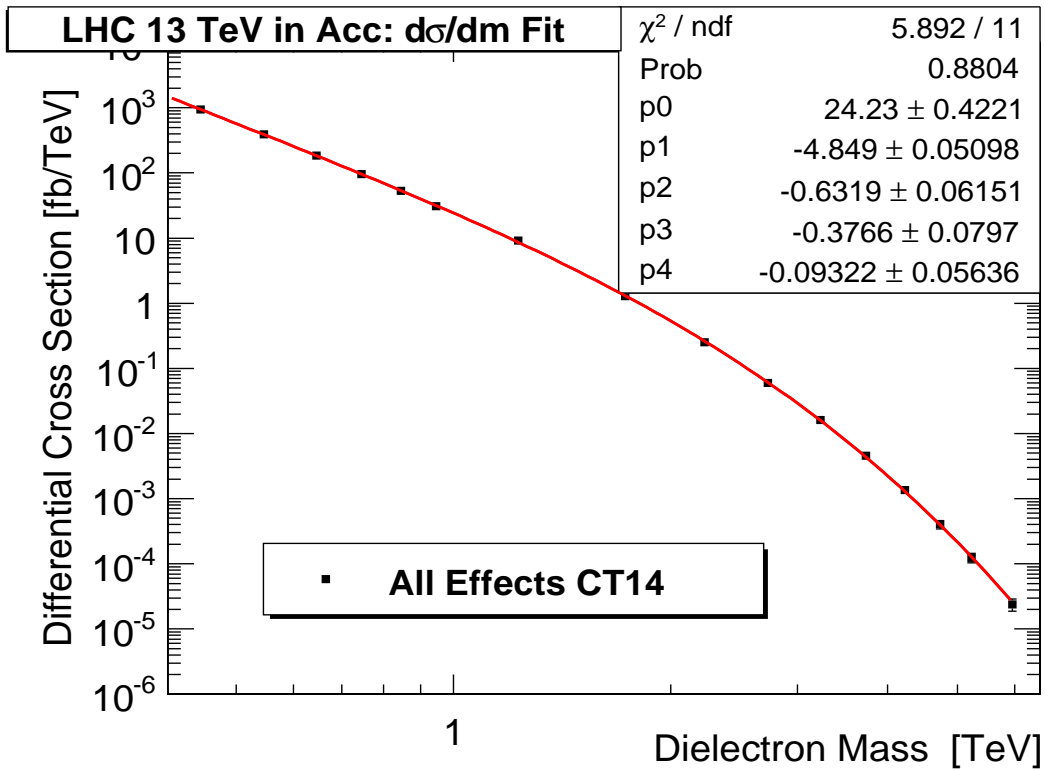


Figure 11: Top: Fit to the differential cross section including all effects (NNLO and PI) for the the dielectron channel. Bottom: Fit to the differential cross section including all effects (NNLO and PI) for the dimuon channel. The CT14 PDF sets are used.

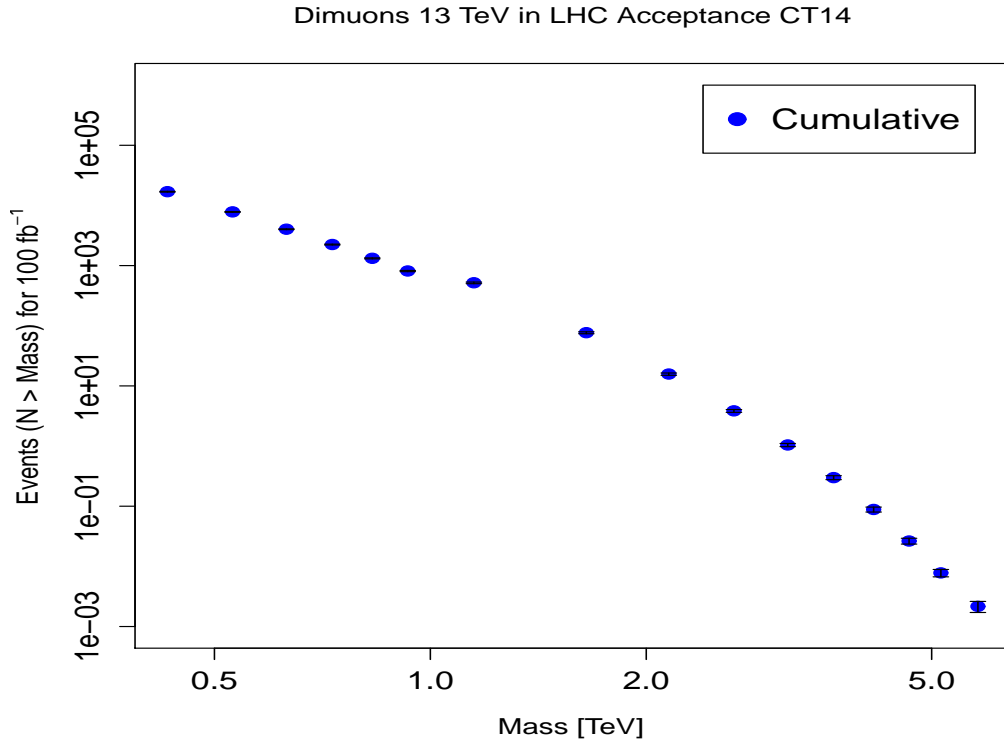
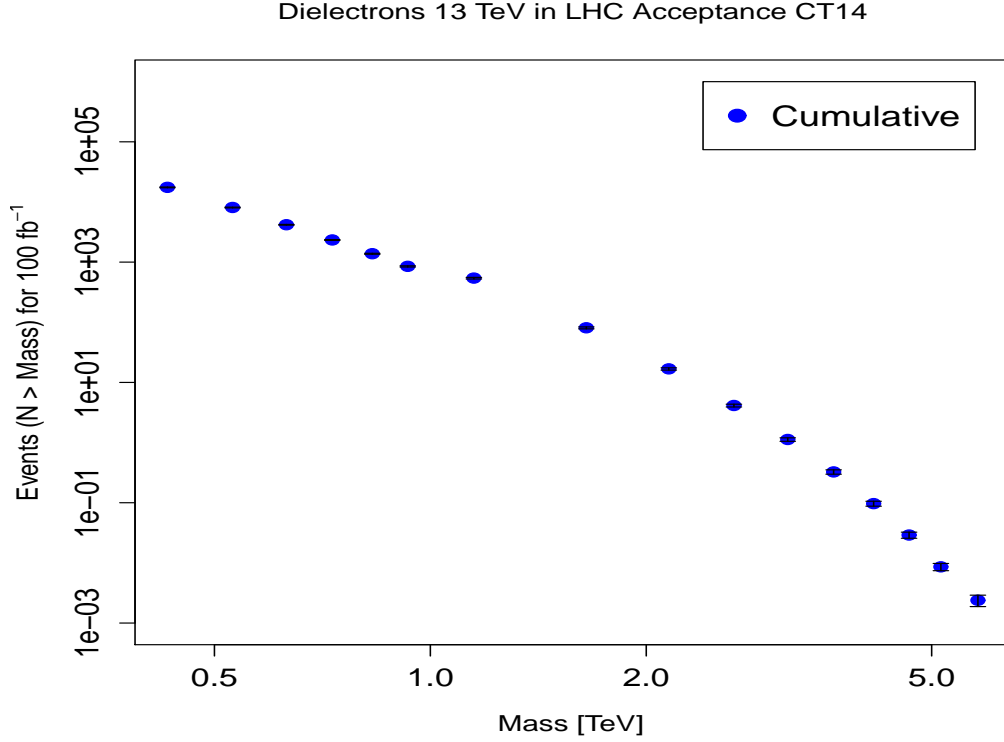


Figure 12: Top: Cumulative number of events expected in one experiment above a given mass for integrated luminosity of 100 fb^{-1} including all effects (NNLO and PI) for the dielectron channel. Bottom: Cumulative number of events expected in one experiment above a given mass for integrated luminosity of 100 fb^{-1} including all effects (NNLO and PI) for the dimuon channel.

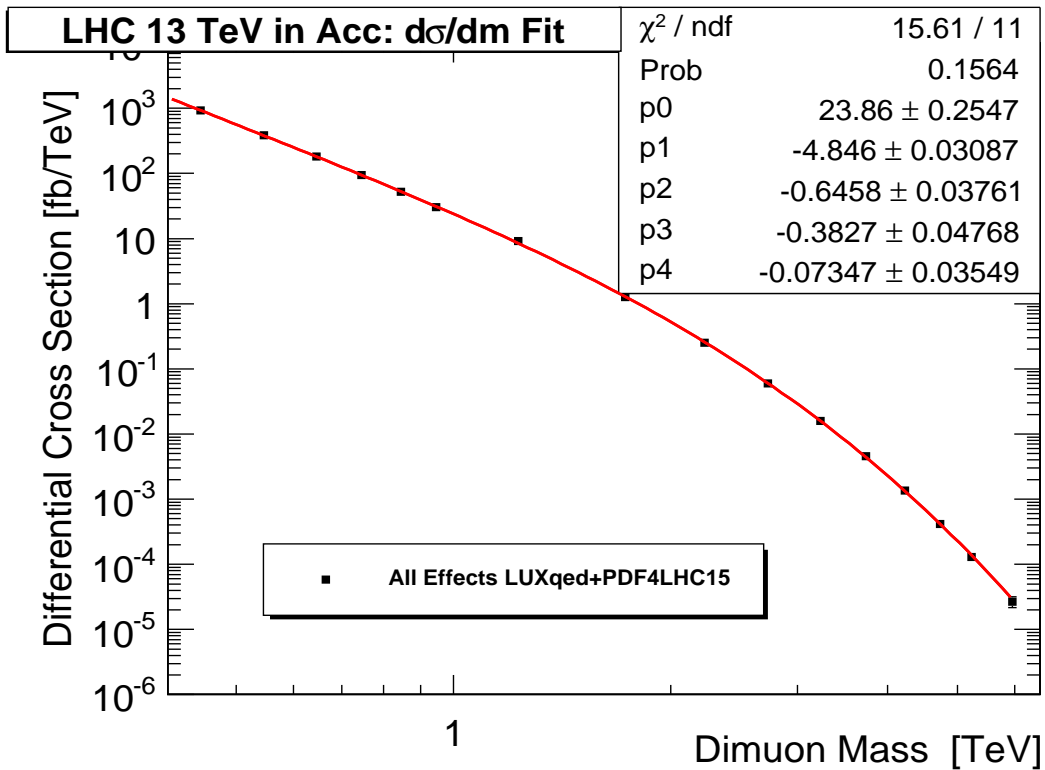
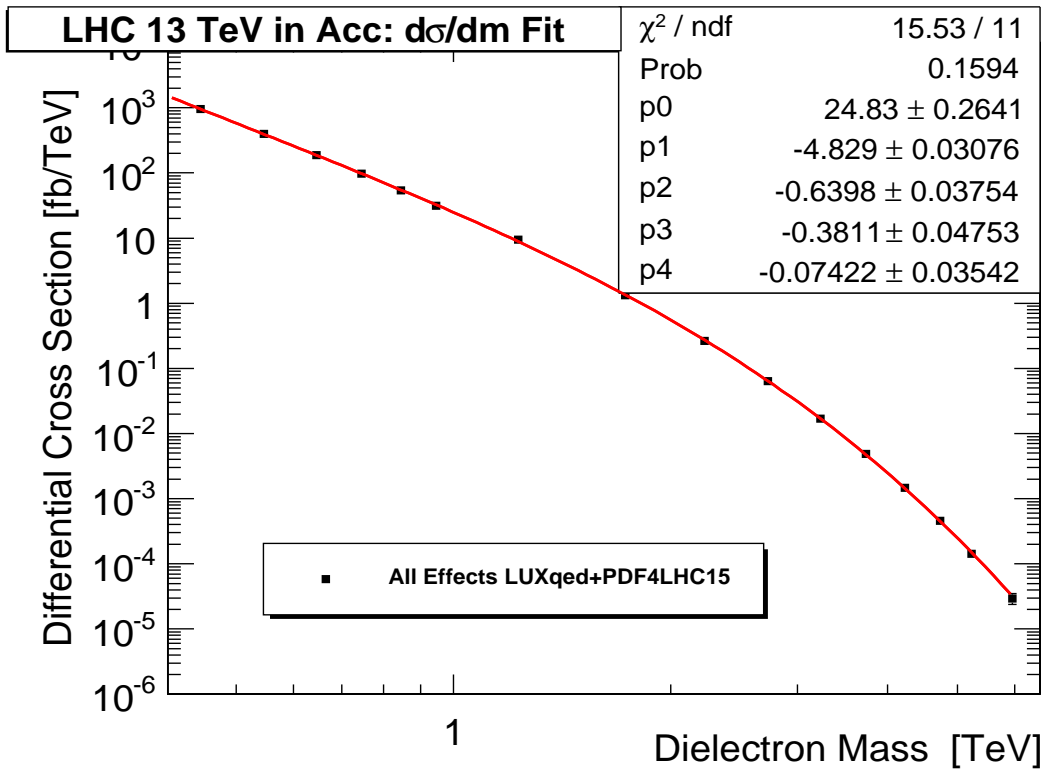


Figure 13: Top: fit to the differential cross section including all effects (NNLO and PI) for the dielectron channel. Bottom: fit to the differential cross section including all effects (NNLO and PI) for the dimuon channel. The LUXqed_plus_PDF4LHC15 PDF set is used.

References

- [1] S. Chatrchyan *et al.* [CMS Collaboration], “Search for Resonances in the Dilepton Mass Distribution in pp Collisions at $\sqrt{s} = 7$ TeV,” JHEP **1105** (2011) 093 doi:10.1007/JHEP05(2011)093 [arXiv:1103.0981 [hep-ex]].
- [2] V. Khachatryan *et al.* [CMS Collaboration], “Search for physics beyond the standard model in dilepton mass spectra in proton-proton collisions at $\sqrt{s} = 8$ TeV,” JHEP **1504** (2015) 025 doi:10.1007/JHEP04(2015)025 [arXiv:1412.6302 [hep-ex]].
- [3] V. Khachatryan *et al.* [CMS Collaboration], “Search for narrow resonances in dilepton mass spectra in proton-proton collisions at $\sqrt{s} = 13$ TeV and combination with 8 TeV data,” arXiv:1609.05391 [hep-ex].
- [4] CMS Collaboration [CMS Collaboration], “Search for a high-mass resonance decaying into a dilepton final state in 13 fb^{-1} of pp collisions at $\sqrt{s} = 13$ TeV,” CMS-PAS-EXO-16-031.
- [5] G. Aad *et al.* [ATLAS Collaboration], “Search for high-mass dilepton resonances in pp collisions at $\sqrt{s} = 8$ TeV with the ATLAS detector,” Phys. Rev. D **90** (2014) no.5, 052005 doi:10.1103/PhysRevD.90.052005 [arXiv:1405.4123 [hep-ex]].
- [6] G. Aad *et al.* [ATLAS Collaboration], “Search for contact interactions and large extra dimensions in the dilepton channel using proton-proton collisions at $\sqrt{s} = 8$ TeV with the ATLAS detector,” Eur. Phys. J. C **74** (2014) no.12, 3134 doi:10.1140/epjc/s10052-014-3134-6 [arXiv:1407.2410 [hep-ex]].
- [7] M. Aaboud *et al.* [ATLAS Collaboration], “Search for high-mass new phenomena in the dilepton final state using proton-proton collisions at $\sqrt{s} = 13$ TeV with the ATLAS detector,” Phys. Lett. B **761** (2016) 372 doi:10.1016/j.physletb.2016.08.055 [arXiv:1607.03669 [hep-ex]].
- [8] The ATLAS collaboration [ATLAS Collaboration], “Search for new high-mass resonances in the dilepton final state using proton-proton collisions at $\sqrt{s} = 13$ TeV with the ATLAS detector,” ATLAS-CONF-2016-045.
- [9] S. Schael *et al.* [ALEPH and DELPHI and L3 and OPAL and LEP Electroweak Collaborations], “Electroweak Measurements in Electron-Positron Collisions at W-Boson-Pair Energies at LEP,” Phys. Rept. **532** (2013) 119 doi:10.1016/j.physrep.2013.07.004 [arXiv:1302.3415 [hep-ex]].
- [10] D. Bourilkov, “Two fermion and two photon final states at LEP-2 and search for extra dimensions,” hep-ex/0103039.
- [11] D. Bourilkov, “Fermion pair production above the Z and search for new phenomena,” hep-ex/9806027.
- [12] S. Dulat *et al.*, “New parton distribution functions from a global analysis of quantum chromodynamics,” Phys. Rev. D **93** (2016) no.3, 033006 doi:10.1103/PhysRevD.93.033006 [arXiv:1506.07443 [hep-ph]].

- [13] L. A. Harland-Lang, A. D. Martin, P. Motylinski and R. S. Thorne, “Parton distributions in the LHC era: MMHT 2014 PDFs,” *Eur. Phys. J. C* **75** (2015) no.5, 204 doi:10.1140/epjc/s10052-015-3397-6 [arXiv:1412.3989 [hep-ph]].
- [14] R. D. Ball *et al.* [NNPDF Collaboration], “Parton distributions for the LHC Run II,” *JHEP* **1504** (2015) 040 doi:10.1007/JHEP04(2015)040 [arXiv:1410.8849 [hep-ph]].
- [15] A. Manohar, P. Nason, G. P. Salam and G. Zanderighi, “How bright is the proton? A precise determination of the photon PDF,” arXiv:1607.04266 [hep-ph].
- [16] J. Butterworth *et al.*, “PDF4LHC recommendations for LHC Run II,” *J. Phys. G* **43** (2016) 023001 doi:10.1088/0954-3899/43/2/023001 [arXiv:1510.03865 [hep-ph]].
- [17] D. Bourilkov, R. C. Group and M. R. Whalley, “LHAPDF: PDF use from the Tevatron to the LHC,” hep-ph/0605240.
- [18] C. Schmidt, J. Pumplin, D. Stump and C.-P. Yuan, “CT14QED PDFs from Isolated Photon Production in Deep Inelastic Scattering,” arXiv:1509.02905 [hep-ph].
- [19] S. Alioli *et al.*, “Precision Studies of Observables in $pp \rightarrow W \rightarrow \ell\nu$ and $pp \rightarrow \gamma, Z \rightarrow \ell^+\ell^-$ processes at the LHC,” [arXiv:1606.02330 [hep-ph]].
- [20] Y. Li and F. Petriello, “Combining QCD and electroweak corrections to dilepton production in FEWZ,” *Phys. Rev. D* **86** (2012) 094034 doi:10.1103/PhysRevD.86.094034 [arXiv:1208.5967 [hep-ph]].
- [21] M. R. Whalley, D. Bourilkov and R. C. Group, “The Les Houches accord PDFs (LHAPDF) and LHAGLUE,” hep-ph/0508110.
- [22] D. Bourilkov, “Study of parton density function uncertainties with LHAPDF and PYTHIA at LHC,” hep-ph/0305126.
- [23] A. Buckley, J. Ferrando, S. Lloyd, K. Nordström, B. Page, M. Rfenacht, M. Schnherr and G. Watt, “LHAPDF6: parton density access in the LHC precision era,” *Eur. Phys. J. C* **75** (2015) 132 doi:10.1140/epjc/s10052-015-3318-8 [arXiv:1412.7420 [hep-ph]].
- [24] S. Chekanov *et al.* [ZEUS Collaboration], “Measurement of isolated photon production in deep inelastic ep scattering,” *Phys. Lett. B* **687** (2010) 16 doi:10.1016/j.physletb.2010.02.045 [arXiv:0909.4223 [hep-ex]].
- [25] S. Chatrchyan *et al.* [CMS Collaboration], “Exclusive photon-photon production of muon pairs in proton-proton collisions at $\sqrt{s} = 7$ TeV,” *JHEP* **1201** (2012) 052 doi:10.1007/JHEP01(2012)052 [arXiv:1111.5536 [hep-ex]].
- [26] V. Khachatryan *et al.* [CMS Collaboration], “Evidence for exclusive gamma-gamma to $W^+ W^-$ production and constraints on anomalous quartic gauge couplings at $\sqrt{s} = 7$ and 8 TeV,” arXiv:1604.04464 [hep-ex].
- [27] M. Ababekri, S. Dulat, J. Isaacson, C. Schmidt and C.-P. Yuan, “Implication of CMS data on photon PDFs,” arXiv:1603.04874 [hep-ph].

- [28] L. A. Harland-Lang, V. A. Khoze and M. G. Ryskin, “Photon-initiated processes at high mass,” arXiv:1607.04635 [hep-ph].
- [29] S. Haywood *et al.*, “Electroweak physics,” In *Geneva 1999, Standard model physics (and more) at the LHC* 117-230 [hep-ph/0003275].
- [30] S. Dittmaier, A. Huss and C. Schwinn, “Dominant mixed QCD-electroweak $O(\alpha_s\alpha)$ corrections to DrellYan processes in the resonance region,” Nucl. Phys. B **904** (2016) 216 doi:10.1016/j.nuclphysb.2016.01.006 [arXiv:1511.08016 [hep-ph]].
- [31] K. A. Olive *et al.* [Particle Data Group Collaboration], “Review of Particle Physics,” Chin. Phys. C **38** (2014) 090001.
- [32] D. Bourilkov, “Photon-induced Background for Dilepton Searches and Measurements in pp Collisions at 13 TeV,” arXiv:1606.00523 [hep-ph].
- [33] A. D. Martin, R. G. Roberts, W. J. Stirling and R. S. Thorne, “Parton distributions incorporating QED contributions,” Eur. Phys. J. C **39** (2005) 155 doi:10.1140/epjc/s2004-02088-7 [hep-ph/0411040].
- [34] R. D. Ball *et al.* [NNPDF Collaboration], “Parton distributions with QED corrections,” Nucl. Phys. B **877** (2013) 290 doi:10.1016/j.nuclphysb.2013.10.010 [arXiv:1308.0598 [hep-ph]].
- [35] V. Bertone and S. Carrazza, “Combining NNPDF3.0 and NNPDF2.3QED through the APFEL evolution code,” arXiv:1606.07130 [hep-ph].
- [36] E. Accomando, J. Fiaschi, F. Hautmann, S. Moretti and C. H. Shepherd-Themistocleous, “Photon-initiated production of a di-lepton final state at the LHC: cross section versus forward-backward asymmetry studies,” arXiv:1606.06646 [hep-ph].